

MoreStyle: Relax Low-frequency Constraint of Fourier-based Image Reconstruction in Generalizable Medical Image Segmentation

Haoyu Zhao¹, Wenhui Dong¹, Rui Yu², Zhou Zhao³,
Du Bo¹, and Yongchao Xu¹(✉)

¹ School of Computer Science, Wuhan University, Hubei, China
yongchao.xu@whu.edu.cn

² University of Louisville, Louisville, USA

³ School of Computer Science, Central China Normal University,
Hubei, China

Abstract. The task of single-source domain generalization (SDG) in medical image segmentation is crucial due to frequent domain shifts in clinical image datasets. To address the challenge of poor generalization across different domains, we introduce a Plug-and-Play module for data augmentation called MoreStyle. MoreStyle diversifies image styles by relaxing low-frequency constraints in Fourier space, guiding the image reconstruction network. With the help of adversarial learning, MoreStyle further expands the style range and pinpoints the most intricate style combinations within latent features. To handle significant style variations, we introduce an uncertainty-weighted loss. This loss emphasizes hard-to-classify pixels resulting only from style shifts while mitigating true hard-to-classify pixels in both MoreStyle-generated and original images. Extensive experiments on two widely used benchmarks demonstrate that the proposed MoreStyle effectively helps to achieve good domain generalization ability, and has the potential to further boost the performance of some state-of-the-art SDG methods.

Keywords: Image segmentation · domain generalization · adversarial data augmentation.

1 Introduction

Deep learning has significantly advanced medical image segmentation but faces challenges when applied across diverse domains. Varying imaging characteristics across healthcare centers, resulting from equipment discrepancies, operator skill levels, and considerations like radiation exposure and imaging time [7,24] leads to images of varied styles, which hinder deploying models in clinical settings.

To address these challenges, many works explore unsupervised domain adaptation (UDA) [10,23] and multi-source domain generalization (MDG) [16,21,12,2]. UDA typically requires access to data from the source domain and the unlabeled target domain. Whereas, MDG necessitates access to data from multiple source

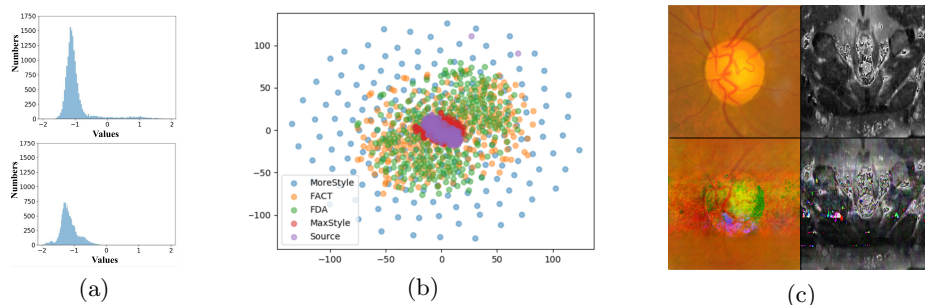


Fig. 1. We adopt the first residual block of pre-trained ResNet-18 [9] to extract image features. (a) Normalized feature distribution on the source images (the upper) and images generated by proposed MoreStyle (the lower). (b) Visualization of feature distribution on the source images and generated images given by methods including MaxStyle [3], FDA [28], FACT [25], and MoreStyle on RIGA+ dataset [1,10,5] with tSNE. (c) Visualization of source image (the upper) and style-augmented images generated by proposed MoreStyle (the lower).

domains. In clinical practice, acquiring target-domain data and redistributing multi-source domain data pose significant challenges due to high costs, privacy, and ethical concerns. Additionally, collecting and annotating extensive datasets is time-consuming, expensive, and sometimes impractical.

Single-source domain generalization (SDG) is a more realistic yet challenging setting where a model is trained exclusively on data from one source domain and then deployed to segment data in unseen target domains. Various methods [4,11,14] have been introduced. A straightforward approach to enhance domain robustness is data augmentation [3,20,19,26], which expands the range of the data and constrains the decision boundaries. Many Fourier-based data augmentation methods [22,8,25,27] emerge. They mainly perform Fourier transformations on images and exchange/mixup [29] the low-frequency components of the amplitude to generate style-augmented images. Though randomly exchanging the low-frequency components of the amplitude effectively generates some images, the augmented styles are still very close to that of the source domain. The images generated by our MoreStyle is widely spread across the tSNE space, as shown in Fig. 1 (b).

In this work, we introduce a novel Plug-and-Play module called MoreStyle to address the style shifts across domains. MoreStyle combines an auxiliary reconstruction decoder with an adversarial noise encoder which is to generate perturbations for the reconstruction decoder. This process is supervised by a novel loss in Fourier space to generate images with same structure and of varied styles, as shown in Fig. 1. Furthermore, we propose an uncertainty-weighted loss based on intersection-union between segmentation results to better handle the segmentation of these varied styles, focusing more on MoreStyle-induced style shifts and less on inherently difficult pixels.

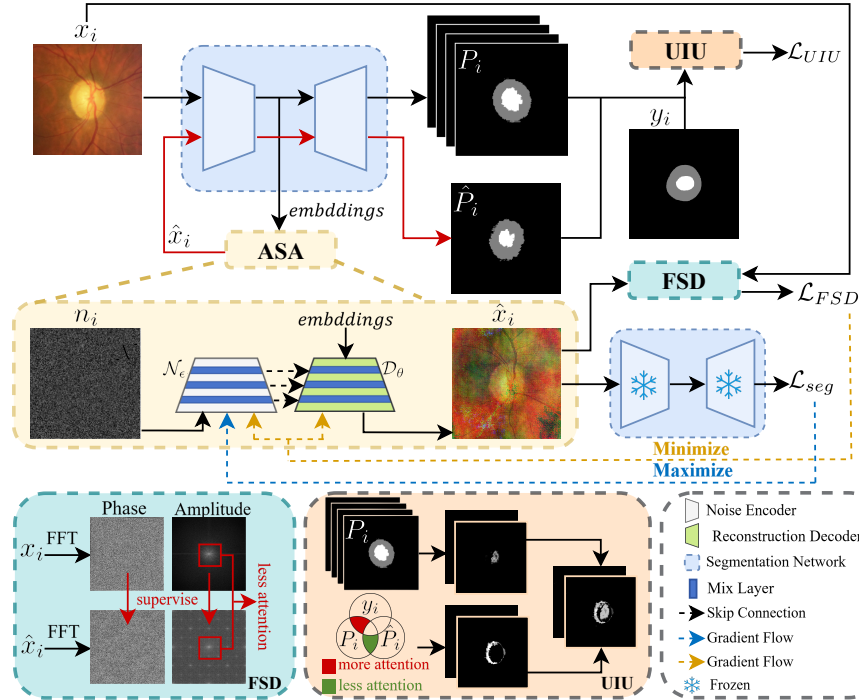


Fig. 2. Pipeline of the proposed MoreStyle. In our proposed MoreStyle framework, we first generate style-augmented images \hat{x}_i using Adversarial Style Augmentation (ASA) and a reconstruction decoder \mathcal{D}_θ , with a noise encoder \mathcal{N}_e generating style mixing γ_i and noise perturbation β_i through adversarial training to affect \mathcal{D}_θ . This image reconstruction is guided by the Fourier Spectrum Diversity (FSD) loss \mathcal{L}_{FSD} . Lastly, both style-augmented \hat{x}_i and source images x_i are input into the segmentation network, supervised by a customized Uncertainty-weighted Intersection-Union (UIU) loss \mathcal{L}_{UIU} .

Our method offers three key contributions: 1) We novelly propose to relax low-frequency constraint in Fourier space between the output of an image reconstruction network and the original image. 2) We propose a customized uncertainty-weighted loss to better deal with hard-to-classify pixels arising from style shifts and pay less attention to the true hard-to-classify pixels for the segmentation network. 3) MoreStyle significantly outperforms some state-of-the-art methods on generalizable OC/OD and prostate segmentation.

2 Method

In this paper, to handle clinical data from unknown domains, we propose a novel Plug-and-Play module called MoreStyle as shown in Fig. 2. We employ an auxiliary reconstruction decoder to generate images of diverse styles, in parallel

with an adversarial noise encoder which generates perturbations for the reconstruction decoder to fail the segmentation network. The source image x_i and generated image \hat{x}_i are utilized to compute Fourier Spectrum Diversity (FSD) loss \mathcal{L}_{FSD} which is to ensure the diversity of the styles of generated images. Furthermore, we employ Uncertainty-weighted Intersection-Union (UIU) loss \mathcal{L}_{UIU} to cope with the diverse styles of generated images $\{\hat{x}_i\}$.

2.1 Adversarial Style Augmentation

Adversarial Style Augmentation (ASA) focuses on generating data samples that fool the segmentation network to improve segmentation robustness. As shown in Fig. 2, ASA involves an auxiliary reconstruction decoder \mathcal{D}_θ and noise encoder \mathcal{N}_ϵ . The noise encoder \mathcal{N}_ϵ generates high-dimensional style mixing γ_i and noise perturbation β_i from noise n_i which is sampled from the Gaussian distribution. High-dimensional noise perturbation and style mixing disturbs the reconstruction decoder \mathcal{D}_θ to generate style-augmented images.

$$\hat{x}_i = \mathcal{D}_\theta(x_i, \beta_i, \gamma_i), \quad (1)$$

where the image x_i is transformed with style mixing γ_i and noise perturbation β_i into style augmented image \hat{x}_i .

Adversarial Training. ASA generates images of varied styles $\{\hat{x}_i\}$ by minimizing \mathcal{L}_{FSD} and maximizing the segmentation loss \mathcal{L}_{seg} . Minimizing \mathcal{L}_{FSD} updates both the noise encoder \mathcal{N}_ϵ and reconstruction decoder \mathcal{D}_θ , encouraging to preserve the structure of the original image x_i for the generated one \hat{x}_i . Maximizing \mathcal{L}_{seg} updates only the noise encoder \mathcal{N}_ϵ , forcing to generate more challenging style mixing γ_i and noise perturbation β_i to disturb the reconstruction decoder, which generates images that fool the segmentation network and thus improves the generalization ability of the segmentation network.

2.2 Fourier Spectrum Diversity Loss

Low-frequency components, containing most of the energy distributions, efficiently capture style variations across diverse domains. In contrast, high-frequency components focus on object structures resembling identity [25,22,18]. Therefore, it is reasonable for the reconstruction decoder \mathcal{D}_θ to pay less attention to the low-frequency components to generate images of diverse styles. To this end, we propose a novel reconstruction loss called Fourier Spectrum Diversity (FSD) loss \mathcal{L}_{FSD} which relaxes the low-frequency constraint in Fourier space.

For an image $x_i \in \mathbb{R}^{H \times W \times C}$, where H , W , C denote the height, width and number of channels, respectively, its frequency space signal $\mathcal{F}(x_i)$ can be obtained with Fast Fourier Transform (FFT), which is defined as follows:

$$\mathcal{F}(x_i)(u, v, c) = \sum_{h=1}^H \sum_{w=1}^W x_i(h, w, c) e^{-j2\pi(\frac{h}{H}u + \frac{w}{W}v)} = \mathcal{A}(x_i) e^{j\mathcal{P}(x_i)}, \quad (2)$$

where $j^2 = -1$, and $\mathcal{A}(x_i)$ and $\mathcal{P}(x_i)$ refer to the amplitude and phase spectra of x_i , respectively. We center the low-frequency components within the frequency spectrum, and then introduce a binary mask $\mathcal{M} \in \mathbb{R}^{H \times W}$, where all values are zero except in the central region. Following [11], the low-frequency components $\mathcal{A}_l(x_i)$ and high-frequency components $\mathcal{A}_h(x_i)$ are given by:

$$\begin{aligned}\mathcal{A}_l(x_i) &= \mathcal{M} \odot \mathcal{A}(x_i), \\ \mathcal{A}_h(x_i) &= (I - \mathcal{M}) \odot \mathcal{A}(x_i),\end{aligned}\tag{3}$$

where \odot denotes element-wise multiplication. The Fourier Spectrum Diversity Loss \mathcal{L}_{FSD} is then defined as follows:

$$\begin{aligned}\mathcal{L}_{FSD}(x_i, \hat{x}_i) &= \mathcal{L}_{mse}(\mathcal{P}(x_i), \mathcal{P}(\hat{x}_i)) + \lambda_1 \mathcal{L}_{mse}(x_i, \hat{x}_i) \\ &+ \lambda_2 \mathcal{L}_{mse}(\mathcal{A}_h(x_i), \mathcal{A}_h(\hat{x}_i)) + \lambda_3 \mathcal{L}_{mse}(\mathcal{A}_l(x_i), \mathcal{A}_l(\hat{x}_i)),\end{aligned}\tag{4}$$

where λ_1 , λ_2 and λ_3 decay exponentially at a rate of 0.99 raised to the power of the epoch number, thereby encouraging \mathcal{D}_θ to generate images of more styles.

2.3 Uncertainty-weighted Intersection-Union Loss

It is crucial to effectively leverage these style-augmented images, therefore, we propose an Uncertainty-weighted Intersection-Union (UIU) loss \mathcal{L}_{UIU} between the segmentation results of original image x_i and generated style-augmented image \hat{x}_i . We pay more attention to the hard-to-classify pixels arising only from style shifts, while giving less emphasis to the common hard-to-classify pixels between the images generated above and the original one.

We identify challenging pixels due to style shifts which are those easily segmented in x_i but problematic in \hat{x}_i . Our aim is to make the network focus more on the hard-to-classify pixels arising only from style shifts $P_i^k \cap y_i^k - P_i^k \cap y_i^k \cap \hat{P}_i^k$ (more attention region in Fig. 2), where k means the k -th class. The collection of these pixels is denoted as m_i . The common hard-to-classify pixels between the images generated above and the original one are $P_i^k \cap \hat{P}_i^k - P_i^k \cap y_i^k \cap \hat{P}_i^k$ (less attention regions in Fig. 2). These pixels are grouped into a set called l_i .

We then estimate pixel-wise uncertainty using the Monte Carlo Dropout method [13,6] to find pixels that pose challenge to network segmentation. We perform T stochastic forward passes through segmentation network using x_i^T which is generated by adding random Gaussian noise on x_i . The uncertainty map u_i is created by calculating the entropy of the predictions, highlighting pixels with high entropy as the most challenging ones. We do not consider \hat{x}_i in this step because it will lead the uncertainty map to emphasize challenging pixels due to immense style variations rather than inherently challenging pixels.

Given uncertainty map u_i and two sets of pixels m_i and l_i , for every pixel in m_i , we enhance its value in u_i by applying a multiplication factor of ρ . Conversely, for pixels within l_i , their values in u_i are adjusted by multiplying with a factor of σ . We set ρ to 1.2 and σ to 0.8 in this paper. Finally, the Uncertainty-weighted Intersection-Union loss \mathcal{L}_{UIU} for i -th image is given by:

$$\mathcal{L}_{UIU}(P_i, y_i) = -\frac{1}{HW} \sum_{j=1}^{HW} w_i^j (y_i^j \log P_i^j + (1 - y_i^j) \log(1 - P_i^j)). \quad (5)$$

The final segmentation loss is defined as $\mathcal{L}_{seg} = \mathcal{L}_{UIU}(P_i, y_i) + \mathcal{L}_{dice}(P_i, y_i)$.

3 Experiments

3.1 Dataset and Training Details

We conduct experiments on two public datasets the RIGA+ dataset⁴ [1,10,5] and the prostate dataset⁵ [16]. In RIGA+ dataset, each image is resized to 512×512 pixels, and we select BinRushed and Magrabia as the source domains to train our segmentation network. In prostate dataset, we preprocess these MRI cases following the methods of a prior study [10], and then resize slices to 384×384 pixels with the same voxel spacing. To evaluate the segmentation performance, we employ the Dice Similarity Coefficient.

In all our experiments, we use the same backbone data augmentation strategy as in [11]. We set λ_2 to 5×10^{-5} , λ_3 to 5×10^{-6} and λ_1 to 5×10^{-3} in Eq. 4. In the reconstruction decoder \mathcal{D}_θ , mix layers are integrated within the first three convolutional blocks and are activated at a probability of 0.5 to introduce feature perturbation. For the noise encoder \mathcal{N}_ϵ , we employ a specific noise optimizer, whereas another optimizer is utilized for both \mathcal{D}_θ and \mathcal{N}_ϵ . We set learning rate to 1×10^{-2} for segmentation network. For MedSAM [17], the learning rate is set to 1×10^{-5} on RIGA+ and 1×10^{-7} on prostate. All experiments are conducted using the PyTorch framework on an NVIDIA 3090 GPU.

3.2 Comparison with State-of-the-art Methods

We conduct comparative experiments against various state-of-the-art (SOTA) methods, including (1) MaxStyle [3] using adversarial noise; (2-4) MixStyle [31], DSU [15] and EFDM [30] with feature-space domain randomization; (5) SLAug [20] applying Bézier transformation to both global and local regions; (6) CCSDG [11] finding invariant between domains; (7) Medical foundation model, MedSAM [17].

As shown in Table 1 and Table 2, MoreStyle yields good results on both datasets. Notably, in comparison with recent methods such as MedSAM [17] and CCSDG [11], the application of MoreStyle yields notable improvement. Some qualitative results are shown in Fig. 3, compared with some SOTA methods, MoreStyle achieves more accurate segmentation result.

Unlike other adversarial data augmentation methods that may need long training times, MoreStyle achieves good results in only 100 epochs, significantly less than the 600 epochs required by MaxStyle [3] for satisfactory outcomes.

⁴ <https://zenodo.org/records/6325549/>

⁵ <http://medicaldecathlon.com/>

Table 1. The experimental results on OC/OD segmentation. The source domains are BinRushed (top 2 groups) and Magrabia (bottom 2 groups), respectively. The target domains are BASE1, BASE2, and BASE3. The best result is in blue.

Method	Base1		Base2		Base3		Avg	
	OC	OD	OC	OD	OC	OD	OC	OD
MixStyle (ICLR2021) [31]	92.59	81.12	89.32	72.90	93.67	78.62	91.84	77.70
DSU (ICLR2022) [15]	91.70	82.63	82.54	70.26	90.15	77.97	88.26	77.23
EFDM (CVPR2022) [30]	93.32	78.20	93.20	79.78	91.34	80.63	92.70	80.63
MaxStyle (MICCAI2022) [3]	95.22	82.49	94.46	79.19	93.96	79.27	94.60	80.47
SLAug (AAAI2023) [20]	93.17	81.18	91.60	77.32	94.77	81.96	93.13	80.15
MoreStyle (Ours)	96.08	85.58	96.20	88.29	96.03	87.11	96.10	86.91
CCSDG (MICCAI2023) [11]	95.45	86.14	95.68	86.42	95.62	85.60	95.57	86.07
CCSDG+MoreStyle	95.70	86.30	96.08	86.91	95.55	86.06	95.78	86.42
MedSAM (Nat. Commun2024) [17]	94.15	82.19	93.42	86.55	94.00	83.39	93.87	83.96
MedSAM+MoreStyle	94.62	84.62	94.77	86.14	94.48	84.64	94.63	85.12
MixStyle (ICLR2021) [31]	93.76	80.26	92.93	78.65	90.94	82.63	92.66	80.43
DSU (ICLR2022) [15]	93.65	81.62	92.09	77.63	91.40	82.57	92.48	80.60
EFDM (CVPR2022) [30]	93.10	80.84	91.11	78.54	91.70	82.23	92.04	80.50
MaxStyle (MICCAI2022) [3]	94.54	83.24	94.64	85.27	93.99	84.67	94.41	84.32
SLAug (AAAI2023) [20]	92.76	82.07	92.83	81.66	90.94	81.71	92.25	81.83
MoreStyle (Ours)	95.04	87.38	95.63	87.71	95.25	86.16	95.29	87.13
CCSDG (MICCAI2023) [11]	95.15	84.57	95.25	82.17	95.09	83.84	95.16	83.57
CCSDG+MoreStyle	95.11	86.47	95.13	90.10	95.60	87.83	95.26	88.05
MedSAM (Nat. Commun2024) [17]	93.32	69.56	93.96	77.49	93.84	77.36	93.68	74.44
MedSAM+MoreStyle	94.30	73.08	94.38	80.59	93.99	77.53	94.24	76.79

Table 2. The experimental results on prostate segmentation. Each column is the Dice score averaged on the rest domains except the source domain for training.

Method	A to Rest	B to Rest	C to Rest	D to Rest	E to Rest	F to Rest	Avg
MixStyle (ICLR2021) [31]	72.32	64.19	40.27	60.23	40.33	48.59	54.32
DSU (ICLR2022) [15]	73.51	64.85	45.08	64.05	42.27	43.38	55.52
EFDM (CVPR2022) [30]	73.53	64.06	45.49	61.15	41.07	47.45	55.46
MaxStyle (MICCAI2022) [3]	73.40	63.63	51.45	62.15	38.14	56.31	57.51
SLAug (AAAI2023) [20]	79.31	68.47	58.47	68.25	48.88	57.61	63.50
Morestyle (Ours)	80.06	74.42	54.16	65.96	51.12	54.19	63.32
CCSDG (MICCAI2023) [11]	80.62	69.52	65.18	67.89	58.99	63.27	67.58
CCSDG+MoreStyle	80.67	75.99	66.28	69.57	60.38	67.22	70.02
MedSAM (Nat. Commun2024) [17]	88.02	87.92	87.21	88.11	87.42	88.43	87.85
MedSAM+MoreStyle	88.43	88.69	87.47	88.50	88.32	88.59	88.33

Ablation Studies. To evaluate the effectiveness of our proposed modules, including ASA, FSD and UIU, we conduct ablation experiments using RIGA+ dataset [1,10,5]. The corresponding results are shown in Table 3. It reveals that ASA, FSD and UIU all contribute to performance gains. Additional hyperparameter ablation studies are in supplementary materials. MoreStyle increases the number of parameters by 8.6% compared to the baseline. Considering the significant performance improvement over the baseline model **without any extra inference time**, this small amount of extra cost is deserving. It is worth mentioning that different from other DG methods, MoreStyle does not necessarily sacrifice the in-dataset performance, as shown in Table. 3.

Comparison with classic Fourier-based data augmentation methods. ASA+FSD has much better performance than traditional Fourier-based data augmentation such as FDA [28] and FACT [25], as shown in Table 4 and supplementary materials. This indicates that, unlike direct swapping in the Fourier

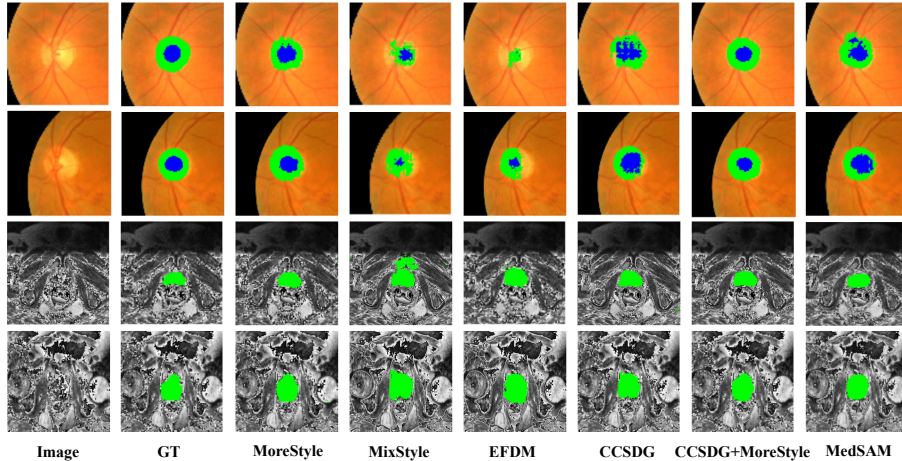


Fig. 3. Visualization of results by MoreStyle and several SOTA methods.

Table 3. Ablation studies on the impact of each module in our method under both in-dataset and cross-dataset settings.

Method	#Params	Average	
		OC	OD
Baseline (cross-dataset)	43.80M	89.12	77.90
Baseline+ASA (cross-dataset)	47.56M	93.11	81.63
Baseline+ASA+FSD (cross-dataset)	47.56M	95.42	86.27
MoreStyle (cross-dataset)	47.56M	95.70	87.02
Baseline (in-dataset)	43.80M	95.64	84.25
MoreStyle (in-dataset)	47.56M	96.10	85.29

Table 4. Comparison between data augmentation in MoreStyle with some classical Fourier-based data augmentations.

Method	Average	
	OC	OD
Baseline	89.12	77.90
Baseline+FDA [28]	94.33	83.81
Baseline+FACT [25]	93.94	82.25
Baseline+ASA+FSD	95.42	86.27

domain, our MoreStyle can generate images of more diverse styles, improving the generalization ability of segmentation network.

4 Conclusion

In this paper, we propose a novel Plug-and-Play module called MoreStyle to significantly enhance the diversity of the training data by relaxing low-frequency constraint in Fourier space to supervise the reconstruction decoder. Combined with adversarial style augmentation, we effectively generate images of diverse styles. We then propose an uncertainty-weighted loss to better make use of these diversely style-augmented images. In particular, on one hand, we propose to pay more attention to hard-to-classify pixels arising only from domain shifts to explore the potential of generated images for segmentation network. On the other hand, we pay less attention to the true hard-to-classify pixels for both the generated and original images to cope with the diversely augmented styles. Extensive experiments on two public datasets demonstrate that the proposed MoreStyle

is effective, significantly/consistently boosting the performance of some state-of-the-art methods. The limitation is that while MoreStyle excels in generating images of various styles, it struggles to generalize effectively to images with geometric variations. Integrating MoreStyle into geometric data augmentation would be an interesting direction.

References

1. Almazroa, et al: Retinal fundus images for glaucoma analysis: the RIGA dataset. In: *Medical Imaging 2018: Imaging Informatics for Healthcare, Research, and Applications*. vol. 10579, pp. 55–62 (2018)
2. Chen, et al: Treasure in distribution: A domain randomization based multi-source domain generalization for 2d medical image segmentation. In: *Proc. of Intl. Conf. on Medical Image Computing and Computer Assisted Intervention*. pp. 89–99 (2023)
3. Chen, C., Li, Z., Ouyang, C., Sinclair, M., Bai, W., Rueckert, D.: Maxstyle: Adversarial style composition for robust medical image segmentation. In: *Proc. of Intl. Conf. on Medical Image Computing and Computer Assisted Intervention*. pp. 151–161 (2022)
4. Cugu, I., Mancini, M., Chen, Y., Akata, Z.: Attention consistency on visual corruptions for single-source domain generalization. In: *Proc. of IEEE Conf. on Computer Vision and Pattern Recognition*. pp. 4165–4174 (2022)
5. Decencière, et al: Feedback on a publicly distributed image database: the Messidor database. *Image Analysis & Stereology* **33**(3), 231–234 (2014)
6. Gal, Y., Ghahramani, Z.: Dropout as a bayesian approximation: Representing model uncertainty in deep learning. In: *Proc. of Intl. Conf. on Machine Learning*. pp. 1050–1059 (2016)
7. Guan, H., Liu, M.: Domain adaptation for medical image analysis: a survey. *IEEE Transactions on Biomedical Engineering* **69**(3), 1173–1185 (2021)
8. Guo, J., Wang, N., Qi, L., Shi, Y.: ALOFT: A lightweight mlp-like architecture with dynamic low-frequency transform for domain generalization. In: *Proc. of IEEE Conf. on Computer Vision and Pattern Recognition*. pp. 24132–24141 (2023)
9. He, K., Zhang, X., Ren, S., Sun, J.: Deep residual learning for image recognition. In: *Proc. of IEEE Conf. on Computer Vision and Pattern Recognition*. pp. 770–778 (2016)
10. Hu, et al: Domain specific convolution and high frequency reconstruction based unsupervised domain adaptation for medical image segmentation. In: *Proc. of Intl. Conf. on Medical Image Computing and Computer Assisted Intervention*. pp. 650–659 (2022)
11. Hu, et al: Devil is in channels: Contrastive single domain generalization for medical image segmentation. In: *Proc. of Intl. Conf. on Medical Image Computing and Computer Assisted Intervention*. pp. 14–23 (2023)
12. Hu, S., Liao, Z., Zhang, J., Xia, Y.: Domain and content adaptive convolution based multi-source domain generalization for medical image segmentation. *IEEE Trans. on Medical Imaging* **42**(1), 233–244 (2022)
13. Kendall, A., Gal, Y.: What uncertainties do we need in bayesian deep learning for computer vision? *Proc. of Advances in Neural Information Processing Systems* pp. 5574–5584 (2017)
14. Li, H., et al: Frequency-mixed single-source domain generalization for medical image segmentation. In: *Proc. of Intl. Conf. on Medical Image Computing and Computer Assisted Intervention*. pp. 127–136 (2023)

15. Li, X., Dai, Y., Ge, Y., Liu, J., Shan, Y., Duan, L.Y.: Uncertainty modeling for out-of-distribution generalization. *Proc. of International Conference on Learning Representations* (2022)
16. Liu, Q., et al.: Ms-net: Multi-site network for improving prostate segmentation with heterogeneous mri data. *IEEE Trans. on Medical Imaging* **39**(9), 2713–2724 (2020)
17. Ma, J., He, Y., Li, F., Han, L., You, C., Wang, B.: Segment anything in medical images. *Nature Communications* **15**(1), 654 (2024)
18. Oppenheim, A., Lim, J.: The importance of phase in signals. *Proceedings of the IEEE* **69**(5), 529–541 (1981)
19. Ouyang, et al: Causality-inspired single-source domain generalization for medical image segmentation. *IEEE Trans. on Medical Imaging* **42**(4), 1095–1106 (2022)
20. Su, et al: Rethinking data augmentation for single-source domain generalization in medical image segmentation. In: *Proc. of the AAAI Conf. on Artificial Intelligence*. vol. 37, pp. 2366–2374 (2023)
21. Wang, J., Lan, C., Liu, C., Ouyang, Y., Qin, T., Lu, W., Chen, Y., Zeng, W., Yu, P.: Generalizing to unseen domains: A survey on domain generalization. *IEEE Transactions on Knowledge and Data Engineering* (2022)
22. Wang, J., Du, R., Chang, D., Liang, K., Ma, Z.: Domain generalization via frequency-domain-based feature disentanglement and interaction. In: *Proceedings of the 30th ACM International Conference on Multimedia*. pp. 4821–4829 (2022)
23. Wilson, G., Cook, D.J.: A survey of unsupervised deep domain adaptation. *ACM Transactions on Intelligent Systems and Technology (TIST)* **11**(5), 1–46 (2020)
24. Xie, X., Niu, J., Liu, X., Chen, Z., Tang, S., Yu, S.: A survey on incorporating domain knowledge into deep learning for medical image analysis. *Medical Image Analysis* **69**, 101985 (2021)
25. Xu, Q., Zhang, R., Zhang, Y., Wang, Y., Tian, Q.: A fourier-based framework for domain generalization. In: *Proc. of IEEE Conf. on Computer Vision and Pattern Recognition*. pp. 14383–14392 (2021)
26. Xu, Y., Xie, S., Reynolds, M., Ragoza, M., Gong, M., Batmanghelich, K.: Adversarial consistency for single domain generalization in medical image segmentation. In: *Proc. of Intl. Conf. on Medical Image Computing and Computer Assisted Intervention*. pp. 671–681 (2022)
27. Yang, Y., Lao, D., Sundaramoorthi, G., Soatto, S.: Phase consistent ecological domain adaptation. In: *Proc. of IEEE Conf. on Computer Vision and Pattern Recognition*. pp. 9011–9020 (2020)
28. Yang, Y., Soatto, S.: Fda: Fourier domain adaptation for semantic segmentation. In: *Proc. of IEEE Conf. on Computer Vision and Pattern Recognition*. pp. 4085–4095 (2020)
29. Zhang, H., Cisse, M., Dauphin, Y.N., Lopez-Paz, D.: mixup: Beyond empirical risk minimization. *Proc. of International Conference on Learning Representations* (2018)
30. Zhang, Y., Li, M., Li, R., Jia, K., Zhang, L.: Exact feature distribution matching for arbitrary style transfer and domain generalization. In: *Proc. of IEEE Conf. on Computer Vision and Pattern Recognition*. pp. 8035–8045 (2022)
31. Zhou, K., Yang, Y., Qiao, Y., Xiang, T.: Domain generalization with mixstyle. *Proc. of International Conference on Learning Representations* (2021)

Supplementary Materials

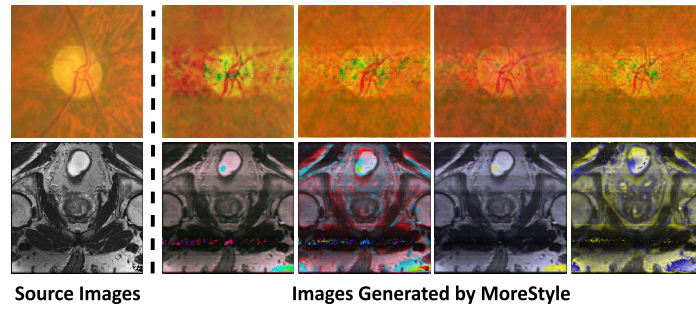


Fig. 1. Illustration of style-augmented images generated by the proposed MoreStyle.

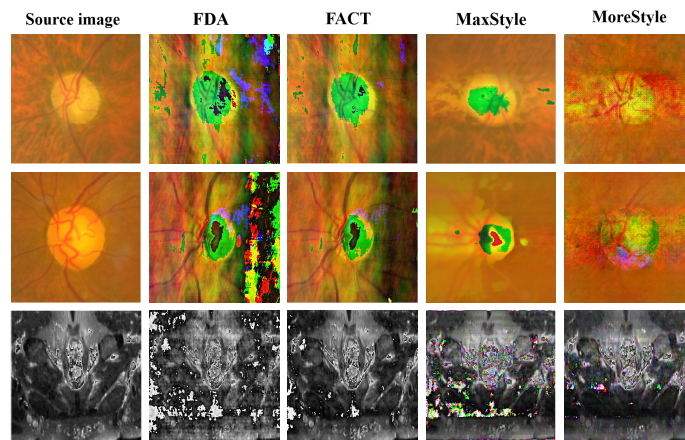


Fig. 2. Qualitative comparison of style-augmented images generated by FDA, FACT, MaxStyle and proposed MoreStyle. Due to the single-channel nature of the prostate images, for a better visualization, we create color images by overlaying three generated images into RGB channel.

Table 1. Ablation study on the impact of λ_1 , λ_2 and λ_3 in Eq. 4, ρ and σ in Sec. 2.3 and number of mix layers on RIGA+. We set λ_1 to 5×10^{-3} , ρ to 0.8, σ to 1.2 and number of layers to 3 in our paper. The best result is **bold**.

Method	BinRushed		Magrabia	
	OC	OD	OC	OD
$\lambda_1 = 5 \times 10^{-2}$	94.57	77.96	92.80	80.42
$\lambda_1 = 5 \times 10^{-3}$	96.10	86.91	95.29	87.13
$\lambda_1 = 5 \times 10^{-4}$	94.06	80.81	93.00	82.57
$\lambda_2 = 5 \times 10^{-4}, \lambda_3 = 5 \times 10^{-5}$	90.76	74.63	89.67	74.81
$\lambda_2 = 5 \times 10^{-5}, \lambda_3 = 5 \times 10^{-6}$	96.10	86.91	95.29	87.13
$\lambda_2 = 5 \times 10^{-6}, \lambda_3 = 5 \times 10^{-7}$	92.93	77.82	85.59	78.15
$\rho=0.5, \sigma=2$	94.37	83.61	92.61	81.64
$\rho=0.8, \sigma=1.2$	96.10	86.91	95.29	87.13
$\rho=1, \sigma=1$	95.89	86.67	94.94	85.87
Number of layers =2	92.78	82.83	92.79	79.96
Number of layers =3	96.10	86.91	95.29	87.13
Number of layers =4	94.51	82.84	93.68	84.08